IEEE Access
Multidisciplinary | Rapid Review | Open Access Journal

Received March 8, 2019, accepted March 30, 2019, date of publication April 9, 2019, date of current version April 18, 2019.

Digital Object Identifier 10.1109/ACCESS.2019.2909738

Photonic Generation and Transmission of Linearly Chirped Microwave Waveform With Increased Time-Bandwidth Product

KUN ZHANG[1,2], SHANGHONG ZHAO[1], YUFU YIN[1], TAO LIN[1], XUAN LI[1], WEI JIANG[1,2], AND GUODONG WANG[1]

[1]Information and Navigation College, Air Force Engineering University, Xi'an 710077, China
[2]National Key Laboratory of Science and Technology on Space Microwave, Xi'an 710000, China

Corresponding author: Kun Zhang (zhangkunyyd@163.com)

This work was supported in part by the National Natural Science Foundation of China under Grant 61571461, Grant 61401502, and Grant 61231012, and in part by the Natural Science Foundation of Shaanxi Province under Grant 2016JQ6008.

ABSTRACT Photonic generation and transmission of linearly chirped microwave waveform with the increased time-bandwidth product (TBWP) is proposed and demonstrated by phase-encoding and splitting parabolic waveform. In the approach, dual-polarization Mach–Zehnder modulator (DPol-MZM) along with polarization controller (PC) is employed to generate two orthogonally polarized wavelengths, and polarization modulator is driven by a parabolic signal. After splitting parabolic waveform and convolving with a binary pseudo random sequence, chirped microwave waveform with high bandwidth and large temporal duration is generated, corresponding to an improved TBWP. Dispersion-induced power fading can be effectively avoided in the approach, and chirped signal with constant initial phase can be achieved by adjusting the PC. The proposed approach is verified by simulations. Linearly chirped microwave waveform with the central frequency of 40 GHz, bandwidth of 12.5 GHz, and TBWP of 20 160 is generated. RF spurious suppression ratios of the generated signal are investigated, and pulse compression performances are also analyzed. The system features filter-free, high tunability, compact structure, and large TBWP, which has potential application in the modern radar system.

INDEX TERMS Chirped microwave waveform, time-bandwidth product, microwave photonics, radar pulse compression.

I. INTRODUCTION

Linearly chirped signal, also known as linear frequency modulation signal has been widely investigated for pulse compression in modern radar system. The pulse compression performance of the chirped signal is proportional to the time-bandwidth product (TBWP) [1], [2]. Linearly chirped microwave waveform with increased TBWP can effectively overcome the contradiction between detection range and range resolution [3], [4]. Traditionally, chirped signals are generated in analog or digital circuit, but with the limited bandwidth, low carrier frequency and complicated configuration [5], [6]. To remedy this problem, photonic approaches for chirped signal generation have been proposed, offering advantages such as wide frequency tunability, low phase noise, high frequency process, and electromagnetic interference immunity [7]–[8].

One widely-adopted approach is direct space-to-time (DST) mapping [9]–[11]. Arrayed waveguide array (AWG) [9], free-space components [10] or fiber Bragg grating (FBG) array [11] can be employed to achieve DST mapping. As the shaping pulse is sent into photodetector (PD) for square-law detection, chirped microwave waveform will be obtained. The major limitations are the poor stability and low reconfigurability. To solve this problem, a simple and compact structure base on optically injected semiconductor laser is proposed to increase the TBWP [12]. For the usage of slave and master lasers, the approach may suffer from the high phase noise limitation. Another signal generator based on spectral shaping with wavelength-to-time mapping (SS-WTT) is conducted by using dispersion elements, such as waveguide optics and single-mode fiber (SMF) [13]–[15]. SS-WTT manipulates the spectra of the optical pulse, and

The associate editor coordinating the review of this manuscript and approving it for publication was Nianqiang Li.

dispersion elements map the shaping spectra into time domain. After PD, chirped signal with high central-frequency can be generated. But the time duration of the system is always limited to several nanoseconds, corresponding to a low TBWP (about 100).

As an improvement, optical interferometric configurations are investigated to generate chirped signal with increased TBWP [16], [17]. But separated optical paths make the system sensitive to environment, and the maximal TBWP is limited to the pulse shaper. Another improved approach is conducted by introducing a parabolic phase difference to two separated wavelengths [18]–[23]. In [18], [19], phase modulators (PM) are employed to introduce the parabolic phase difference, after detection in PD, chirped signals with high frequency are obtained, but spatially separated structures make the generated signal with phase jitter problem. In [20], phase-coded approach is proposed to enhance the time duration of the chirped waveform. After phase-encoding with pseudo-random sequence, chirped signal with TBWP up to 80,000 is generated. But the system is complicated and costly for the usage of the mode locked laser (MLL), and the central-frequency is fixed. In [21], optoelectronic oscillator (OEO) is used to generate frequency-tunable optical sidebands, and binary-coded parabolic signals are applied to drive the polarization modulators (PolM). After PD, frequency-tunable chirped signal with increased TBWP can be generated, but the system lacks frequency multiplying operation. On the other hand, TBWP can also be enhanced by splitting parabolic waveform [22]–[23]. In the structures, PolM1 following by an optical bandpass filter is employed to generate orthogonally-polarized wavelengths. Then, the parabolic signal is split into N piece and applied to drive PolM2. After heterodyning detection in PD, the bandwidth of the generated chirp waveform is further increased, while the time duration remains unchanged, corresponding to a large TBWP signal generation. But the carrier frequency is limited to the input RF signal and optical filters make the systems poor tunability.

In this paper, we propose a photonic approach to generate the chirped microwave waveform with increased TBWP by phase-encoding and splitting parabolic waveform. Since the structure is filter-free, the system has the advantages of simple structure, flexible tunability and good integration ability. In the approach, dual-polarization Mach-Zehnder modulator (DPol-MZM) along with polarization controller (PC) are employed to generate two orthogonally-polarized wavelengths, and PolM is driven by the parabolic microwave waveform. After polarization coupling and photoelectric conversion, chirped microwave waveform with double frequency is generated. To increase the TBWP, parabolic waveform is spilt to improve the bandwidth and phase-encoded to improve the temporal duration. Then, chirped signals with high carrier-frequency, long temporal-duration and large bandwidth are generated in the structure. Besides, the system effectively avoids dispersion-induced power fading. The key advantages are the usage of photonic approach to perform four functions simultaneously, 1) generating chirped signal with large TBWP, 2) realizing independent tunability of time duration and bandwidth, 3) conducting frequency multiplying operation, 4) guaranteeing constant initial phase in remote fiber transmission. Chirped signals with large TBWP feature good pulse compression ratio (PCR) and peak-to-sidelobe ratio (PSR), which have potential application in modern radar system.

II. THEORY AND PRINCIPLE

Fig.1 shows the schematic configuration of the chirped microwave generator. A lightwave from the LD is introduced into a DPol-MZM via PC1. DPol-MZM is an integrated device, which is consisting of two sub-MZMs, a polarization beam combiner, and a 90° polarization rotator (PR) [24]. The DPol-MZM is driven by a RF waveform and the PolM is driven by a parabolic waveform, respectively. After a fiber transmission, the Pol is employed to couple the two orthogonally-polarized lightwaves and a PD is employed to perform square-law detection.

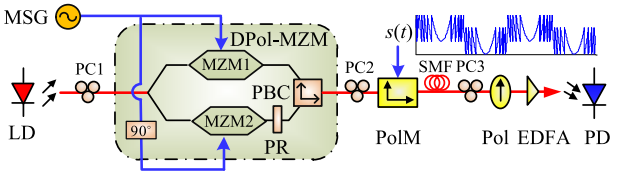

FIGURE 1. Diagram of the proposed chirped microwave waveform generator. LD: laser diode; MSG: microwave signal generator; PC: polarization controller; DPol-MZM: dual-polarization Mach-Zehnder modulator; PR, polarization rotator; PolM: polarization modulator; Pol: polarizer; EDFA: Erbium doped fiber amplifier; PD: photodetector.

In the scheme, the two sub-MZMs are all set to bias at minimum transmission point (MITP). For simplicity, the two sub-MZMs have identical parameters. Adjusting the sinusoidal microwave with a phase gap of 90 degree, the optical fields of the two sub-MZMs can be expressed as:

$$\begin{bmatrix} E_1(t) \\ E_2(t) \end{bmatrix} = E_{in}(t) \begin{bmatrix} \cos\left[\pi V_{RF}/2V_{\pi 1} \cos(2\pi f_{RF} t) + \pi/2\right] \\ \cos\left[\pi V_{RF}/2V_{\pi 1} \sin(2\pi f_{RF} t) + \pi/2\right] \end{bmatrix} \tag{1}$$

where $E_{in}(t) = E_0 \exp(j2\pi f_0 t)$ is the expression of the optical carrier, E_0 and f_0 are the amplitude and carrier frequency of the lightwave, V_{RF} is amplitude of the driven RF signal, $V_{\pi 1}$ is the half-wave voltage of the DPol-MZM. Expanding Eq. (1) with Jacobi-Anger, under small signal condition, Eq.(1) can be approximately expanded as:

$$\begin{bmatrix} E_1(t) \\ E_2(t) \end{bmatrix} \approx J_1(\gamma_1) E_{in}(t) \begin{bmatrix} -\exp(j2\pi f_{RF} t) - \exp(-j2\pi f_{RF} t) \\ j\exp(j2\pi f_{RF} t) - j\exp(-j2\pi f_{RF} t) \end{bmatrix} \tag{2}$$

where $\gamma_1 = \pi V_{RF}/2V_{\pi 1}$ is the modulation index of the DPol-MZM, and $J_n(\cdot)$ is the first nth-order Bessel function. Then the two modulated optical signals are combined with orthogonal polarization states through the PBC. After the

DPol-MZM, PC2 is employed to rotate the polarization direction of the optical signal. The transfer function of the PC2 can be expressed as:

$$T_{PC2} = \begin{bmatrix} \cos\alpha & -\sin\alpha \\ \sin\alpha & \cos\alpha \end{bmatrix} \begin{bmatrix} \exp(j\theta) & 0 \\ 0 & \exp(-j\theta) \end{bmatrix} \quad (3)$$

where α is the polarized rotation angle and θ is the phase difference introduced by the rotation.

Adjusting PC2 to let $\alpha = 45°$ and $\theta = 45°$, the output filed of PC2 can be given as:

$$\begin{bmatrix} E_x(t) \\ E_y(t) \end{bmatrix} = T_{PC2} \begin{bmatrix} E_1(t) \\ E_2(t) \end{bmatrix} \propto \sqrt{2}\, J_1(\gamma_1) E_{in}(t) \times \begin{bmatrix} -\exp(j2\pi f_{RF} t) \\ -\exp(-j2\pi f_{RF} t) \end{bmatrix} \quad (4)$$

From Eq.(4), we can know only first-order sidebands are obtained in the two polarization directions of the PC2. Then the two orthogonally-polarized wavelengths are injected into the PolM, of which two polarization directions have complementary phase modulations. PolM is driven by a parabolic signal $V_s s(t)$, where V_s is the peak voltage and $s(t)$ is the normalized waveform. The optical filed of the PolM can be expressed as:

$$\begin{bmatrix} E_{2x}(t) \\ E_{2y}(t) \end{bmatrix} = \sqrt{2}\, J_1(\gamma_1) E_{in}(t) \begin{bmatrix} -\exp\left[j2\pi f_{RF} t + \gamma_2 s(t)\right] \\ -\exp\left[-j2\pi f_{RF} t - \gamma_2 s(t)\right] \end{bmatrix} \quad (5)$$

where $\gamma_2 = \pi V_s / 2V_{\pi 2}$ is the modulation index of the PolM, $V_{\pi 2}$ is the half-wave voltage of the PolM. In back-to-back condition, the two orthogonally-polarized lightwaves are combined through Pol and sent into PD for heterodyne detection. The AC term of PD can be given as:

$$i_1(t) \propto 4\eta J_1^2(\gamma_1) \cos\left[4\pi f_{RF} t + 2\gamma_2 s(t)\right] \quad (6)$$

where η donates the responsivity of the PD. As a result, the generated current is phase-modulated by $s(t)$. According to the differential relationship between the frequency and phase, a chirped signal can be obtained after a parabolic waveform $s(t)$ is adopted.

Mathematically, a parabolic signal with normalized waveform can be given as:

$$s_1(t) = k(t - T_0/2)^2, t \in [0, T_0] \quad (7)$$

where $k = 4/T_0^2$ $k = 4/\mathrm{T}_0^2 k = 4/\mathrm{T}_0^2 k = 4/\mathrm{T}_0^2$ is the normalization index and T_0 is temporal duration. The bandwidth of the parabolic signal is calculated to $4/T_0$.The waveform of the $s_1(t)$ is shown in Fig. 2(a). Substituting Eq. (7) into Eq. (6), the instantaneous frequency can be calculated as:

$$f_i = 2f_{RF} + \frac{4V_s}{T_0^2 V_{\pi 2}}(t - \frac{T_0}{2}), \quad t \in [0, T_0] \quad (8)$$

Obvious, the generated chirp signal has a central frequency of $2f_{RF}$, chirp rate of $C_1 = 4V_s/T_0^2 V_{\pi 2}$, and bandwidth of $B_1 = 4V_s/T_0 V_{\pi 2}$. The TBWP of the generated signal can be calculated as:

$$TBWP_1 = \frac{4V_s}{V_{\pi 2}} \quad (9)$$

In modern radar observation scene, the chirped signal with large TBWP is necessary [25]. For the existing PloM, the half-wave voltage is a fixed value. From Eq. (9), increased TBWP can only be obtained by employing a parabolic signal with larger peak voltage, while the maximum tolerable electrical power of the PolM is always limited. Therefore, in order to increase the TBWP of the chirped signal, conventional parabolic signal is not acceptable. New methods must be used to increase the time width and bandwidth simultaneously. Besides, remote fiber transmission will bring serious dispersion problems, especially for chirped signal with large TBWP, which must be analyzed and solved [26].

Furthermore, in the structure, PC2 rotates the polarization direction with 45° to obtain two orthogonally-polarized wavelengths, which is the key technology. In practice, rotation phase can be easily adjusted while the polarized rotation angle is hard to control. To verify the stability of the proposed system, assuming there is a $\Delta\alpha$ polarization drift to 45°, Eq. (3) can be rewritten as:

$$T_{PC2} = \begin{bmatrix} \cos(\alpha + \Delta\alpha) & -\sin(\alpha + \Delta\alpha) \\ \sin(\alpha + \Delta\alpha) & \cos(\alpha + \Delta\alpha) \end{bmatrix} \times \begin{bmatrix} \exp(j\theta) & 0 \\ 0 & \exp(-j\theta) \end{bmatrix} \quad (10)$$

Substituting $\mathrm{T}_{\mathrm{PC2}}$ in Eq. (4) with Eq. (10), the output filed of PC2 can be given as:

$$\begin{bmatrix} E_x(t) \\ E_y(t) \end{bmatrix} \propto J_1(\gamma_1) E_{in}(t) \times \begin{bmatrix} \exp(j2\pi f_{RF} t)\cos\Delta a - \exp(-j2\pi f_{RF} t)\sin\Delta a \\ \exp(j2\pi f_{RF} t)\sin\Delta a + \exp(-j2\pi f_{RF} t)\cos\Delta a \end{bmatrix} \quad (11)$$

Polarization extinction ratio (PER) is defined to verify the performance of the generated orthogonally-polarized wavelengths. As can be seen, the PER in Eq.(11) is equal to -20logtan($\Delta\alpha$). Since polarization error $\Delta\alpha$ is usually less than 5°, two orthogonally-polarized wavelengths with PER more than 21.1 dB can be obtained. Besides, as the wavelength is introduced into the PolM for polarized modulation and PD for square-law detection, the AC term of PD can be given as:

$$i_1(t) \propto 4\eta J_1^2(\gamma_1) \left\{ \begin{matrix} \cos\left[4\pi f_{RF} t + 2\gamma_2 s(t)\right]\cos^2(\Delta\alpha) - \\ \cos\left[4\pi f_{RF} t - 2\gamma_2 s(t)\right]\sin^2(\Delta\alpha) \end{matrix} \right\} \quad (12)$$

For the polarization error $\Delta\alpha$, spurious signal appears in the generated signal. The RF spurious suppression ratio (RFSSR) is -20logtan^2($\Delta\alpha$). As we take $\Delta\alpha$ as large as 5 degree, the RFSSR is calculated to 42.3 dB. Therefore, the proposed structure tolerates the polarization direction error of PC2 and shows good reliability in the chirped signal generation.

A. SPLITTING PARABOLIC SIGNAL

To increase the bandwidth of the chirped signal, conventional parabolic signal can be split into N pieces, and the maximum amplitude of each piece is controlled to 1, as shown

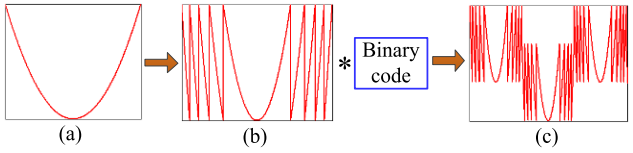

FIGURE 2. Diagram of the input conventional parabolic signal (a), splitting parabolic signal (b), splitting and phase-encoding parabolic signal (c); ∗, convolution operation.

in Fig.2 (b). In this approach, the split parabolic signal can be expressed as:

$$s_2(t) = \frac{N}{2}\begin{cases} k(t - T_0/2)^2 + a_1, 0 \le t < t_1 \\ k(t - T_0/2)^2 + a_2, t_1 \le t < t_2 \\ \cdots \\ k(t - T_0/2)^2 + a_N, t_{N-1} \le t < T_0 \end{cases} \quad (13)$$

where $a_n(n = 1,2,\ldots,N)$ is the value to make each split piece to the same peak voltage and a_n can be calculated to $Nk(t_{n-1}\text{-}T_0/2)^2/2$. The instantaneous frequency of the generated signal is proportional to the differential of $s_2(t)$. Since a_n is a time-independent constant, the values have no effect on the instantaneous frequency. As driving PolM with $V_s s_2(t)$, the bandwidth B_2 of the generated signal is increased to $2NV_s/T_0V_{\pi 2}$, the chirp rate C_2 is increased to $2NV_s/T_0^2V_{\pi 2}$, and the corresponding $TBWP_2$ is:

$$TBWP_2 = \frac{2NV_s}{V_{\pi 2}} \quad (14)$$

Compared with conventional parabolic signal, the TBWP increases N/2-fold. A large TBWP can be obtained by splitting parabolic signal into more pieces. As radar system needs a chirped signal with a constant bandwidth and a large TBWP, the parabolic signal can be stretched N times in the time domain and split into N pieces. Besides, the TBWP can be further improved by employing the RPML-based method [27].

B. SPLITTING AND PHASE-ENCODING

Another solution to improve the TBWP is to increase the temporal duration of the chirped waveform, while controlling the bandwidth fixed [28]. Concerning to this issue, phase-encoding method is proposed, as shown in Fig.2 (c). As the chirped signal has a temporal duration of T_0, chirp rate of C and carrier frequency of f_{RF}, chirped signal can be expressed in time domain as:

$$u_{lfm}(t) = \frac{1}{\sqrt{T_0}} rect(\frac{t}{T_0}) \exp(j2\pi f_{RF} t) \exp(j\pi Ct^2) \quad (15)$$

A phase-coded chirped waveform is usually conducted by a binary pseudo random sequence (BPRS), and a BPRS can be given as:

$$u_b(t) = \begin{cases} \sum_{n=0}^{M-1} c_i \delta(t - nT_0) & 0 \le t < MT_0 \\ 0 & otherwise \end{cases} \quad (16)$$

where M is the sequence length of the BPRS, c_n is the sequence values of the i-th bit, which should be $+1$ or -1.

A phase-coded chirped signal can be calculated by convolving the functions of the BPRS and chirped microwave, which can be expressed as:

$$u_{b-lfm}(t) = u_{lfm}(t) * u_b(t) \quad (17)$$

The convolution operations are implemented in the frequency domain, and the spectra of the phase-coded chirped signal can be given as:

$$U_{b-lfm}(f) = U_{lfm}(f) \times U_b(f) \quad (18)$$

where $U_{lfm}(f)$ and $U_b(f)$ are the Fourier transforms of the chirped signal $u_{lfm}(t)$ and BPRS signal $u_b(t)$. $U_b(f)$ can be calculated as:

$$U_b(f) = FT[u_b(t)] = \frac{1}{T_0}\sum_{n=0}^{M-1} c_n \exp(-j2\pi nT_0 f) \quad (19)$$

Thus, the spectra of the phase-coded chirped signal can be expressed as:

$$U_{b-lfm}(f) = \frac{1}{T_0} U_{lfm} \sum_{n=0}^{M-1} c_n \exp(-j2\pi nT_0 f) \quad (20)$$

From Eq. (20), we can know the bandwidth of the phase-coded chirped signal remains unchanged, while the temporal duration expands M times to the chirped signal. As the proposed generator adopts the splitting parabolic signal, the time duration of the generated signal will increase to MT_0, the bandwidth will increase to $2NV_s/T_0V_{\pi 2}$, the chirp rate will increase to $2NV_s/T_0^2V_{\pi 2}$, and the corresponding TBWP can be calculated as:

$$TBWP_3 = \frac{2NMV_s}{V_{\pi 2}} \quad (21)$$

By splitting and phase-encoding parabolic signal, the TBWP increases by $NM/2$ times. Compared with [21]–[23], our proposed approach can realize independent tunability of time duration and bandwidth by adjusting sequence length M and splitting number N respectively.

C. DISPERSION ANALYSIS IN REMOTE FIBER TRANSMISSION

The proposed approach can generate chirped signal with high frequency and increased TBWP, and show well performance in back-to-back condition. However, in some radar scenarios, central station and antenna are separated, which requires a remote fiber transmission [29], [30]. In our system, the modulated optical signal after PolM has different frequencies in the two polarization directions. Long-distance transmission will bring dispersions problem, which should be analyzed in chirped signal generator.

When the modulated optical signal after PolM propagates a remote base station (BS), a phase shift will be introduced

into the lightwave due to the fiber dispersion. Thence, after a fiber transmission, Eq. (5) can be rewritten as:

$$\begin{bmatrix} E_{3x}(t) \\ E_{3y}(t) \end{bmatrix} = \sqrt{2}\lambda J_1(\gamma_1)E_{in}(t) \times \begin{bmatrix} -\exp j\left[2\pi f_{RF}t + \gamma_2 s(t) + \theta_{+1}\right] \\ -\exp j\left[-2\pi f_{RF}t - \gamma_2 s(t) + \theta_{-1}\right] \end{bmatrix} \quad (22)$$

where E_{3x}(t) and $E_{3y}(t)$ are the optical signals in the two polarization after fiber transmission, $\theta_{+1}$and θ_{-1} are the dispersion phase shifts that are introduced by the upper and the lower sidebands respectively, $\lambda = 10^{-0.05Az}$ is amplitude index, A (dB) is fiber attenuation, and z (Km) is the fiber transmission distance. Expanding propagation constant β at the optical carrier of $2\pi f_0$ in Taylor series [31], we obtain:

$$\begin{cases} \theta_{+1}(\omega) = z\beta(2\pi f_0) + z\beta'(2\pi f_0)f_{RF} + \frac{1}{2}z\beta''(2\pi f_0)2\pi f_{RF}^2 \\ \theta_{-1}(\omega) = z\beta(2\pi f_0) - z\beta'(2\pi f_0)f_{RF} + \frac{1}{2}z\beta''(2\pi f_0)2\pi f_{RF}^2 \end{cases} \quad (23)$$

where $\beta(2\pi f_0)$, $\beta^{'}(2\pi f_0)$ and $\beta^{''}(2\pi f_0)$ are the zeroth-first- and second-order dispersion derivation of propagation constant β. Then the optical transmission signals are introduced into Pol for polarization coupling with 45 degree, and the optical field of the Pol can be given as:

$$E_5(t) = \cos(45^\circ)E_{3x}(t)e^{j\varphi} + \sin(45^\circ)E_{3y}(t)e^{-j\varphi} \quad (24)$$

where φ donates phase difference introduced by PC3 rotation. Finally, the optical signal is sent into PD for heterodyne detection, and AC term of PD can be given as:

$$i_2(t) \propto 4\eta\lambda^2 J_1^2(\gamma_1)\cos \times \left[4\pi f_{RF}t + 2\gamma_2 s(t) + 2z\beta'(2\pi f_0)(2\pi f_{RF}) + 2\varphi\right] \quad (25)$$

The generated current contains carrier frequency term $2f_{RF}$, chirp rate term $2\gamma_2 s(t)$, dispersion term $2z\beta'(2\pi f_0)(2\pi f_{RF})$, and rotation phase term 2φ. Dispersion term and rotation phase term are the time-independent constant, which have no impact on the instantaneous frequency of the generated chirp signal. Therefore, the proposed scheme can realize long-distance fiber transmission, and effectively avoid periodic attenuation of signal power and frequency distortion introduced by fiber dispersion. The power of the generated signal is dependent on the fiber length and fiber attenuation, which can be improved by an EDFA, as shown in Fig.1. Besides, the phase of the generated chirp signal is equal to $2z\beta'(2\pi f_0)(2\pi f_{RF}) + 2\varphi$, which can be freely adjusted by the PC3 rotation.

In the single-center station multi-antenna scenario, the orthogonally-polarized wavelengths are generated by the central station and sent to each base station through the fiber. After polarization controlled in PC3 and detected in PD, chirped signal with high frequency and large TBWP can be generated, which is radiated to free space in each radar antenna and completes detection. As each antenna transmits signals with constant initial phase, the coherent reception of the echo signals can be obtained, and data fusion complexity of echo signals can be reduced. Besides, phase difference φ in the two orthogonal polarization directions can be adjusted by PC3 with 0 to 360 degree. Therefore, the constant initial phase of the antenna radiation signal can always be realized by adjusting PC3:

$$\begin{aligned} &2z_i\beta'(2\pi f_0)(2\pi f_{RF}) + 2\varphi_i = 2k\pi + \phi, \\ &for\ i = 0, 1, 2, \ldots, n \\ &\quad k \in K \end{aligned} \quad (26)$$

where z_i is the distance of the optical fiber, φ_i is the corresponding rotation phase introduced by PC3, ϕ is the fixed initial phase of the antenna, n is the number of the antenna, K donates a positive integer set.

Therefore, frequency-double chirped signal with increased TBWP can be generated by the proposed approach. In the phase-coded chirped signal generator, by tuning the splitting number N of the parabolic signal, the bandwidth of the generated chirp signal can be tuned; by tuning the sequence length M of the BPRS, the temporal duration of the generated chirp signal can be also be tuned; by adjusting the frequency of the RF signal, chirped signal with reconfigurable central-frequency can be generated. Besides, constant initial phase can be realized by adjusting the PC3, which can be used in single-center station multi-antenna scenario.

III. SIMULATION RESULTS AND DISCUSSION

To verify the feasibility of the proposed generator, simulations based on Fig.1 are performed by using Matlab 2014a and OptiSystem 12. The carrier-frequency and power of the LD are set to 193.1 THz and 16 dBm. The DPol-MZM has a half-voltage of 4V, an extinction ratio of 30 dB and an inset loss of 5 dB. The MSG generates sinusoidal waveform with frequency of 20 GHz. The modulation indexes of the DPol-MZM are set to 0.4. The half voltage and inset loss of the PolM are set to 4 V and 5 dB respectively. The erbium doped fiber amplifier (EDFA) has a gain of 18 dB and a noise of 4 dB. The responsivity, dark current and thermal noise of PD are 1 A/W, 10 nA, and 1×10^{-22} W/Hz, respectively.

A. SPLITTING PARABOLIC WAVEFORM

First AWG is employed to generate a normalized parabolic waveform with time duration of 12.8 ns. Then the waveform is amplified with the peak voltage to 6V, and applied to drive the PolM. After modulated in PolM, the optical fields in the two polarization directions are presented in Fig.3. As can be seen, the spectra are expanded due to the parabolic modulation. Besides, for the polarization rotation in PC2, only ±1-st sideband optical wavelengths are left in each polarization direction respectively; for the non-ideal extinction ratio, carrier wavelengths still exist in the two polarization directions.

After Pol with 45 degree, the lightwaves are introduced into PD for square-law detection. The parabolic waveform, spectrum and waveform of the generated current are shown in Fig. 4(a_i-iii). Then the instantaneous frequency is

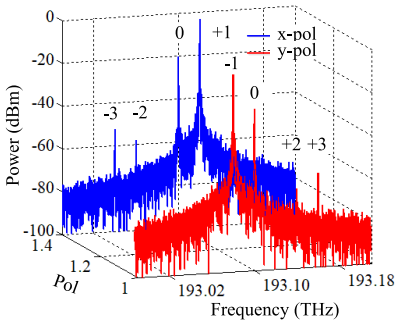

FIGURE 3. Output optical fields of the PolM in the two polarization directions.

extracted by short-time Fourier transform (STFT), as shown in Fig. 4 (a_iv). Thus, chirped waveform with central frequency of 40 GHz, chirp rate of 0.037 GHz/ns, and bandwidth of 0.47 GHz is generated. The TBWP is calculated to 6. The RFSSR is 49.5 dB. To evaluate the pulse compression performance of the generated signal, auto-correlation is investigated, as shown in Fig. 4(a_v). The PSR of the chirped waveform is about 8.55 dB. The full-width at half maximum (FWHM) is 2.63 ns, and the PCR is calculated to 4.87. Besides, in Fig.4 (a_ii), RF signal with carrier frequency of 80 GHz can be further suppressed by employing a low modulation index.

As can be seen in Fig. 4(a), the generated chirp signal has a very limited bandwidth, chirp rate and TBWP. To address this problem, splitting parabolic waveform is investigated. A normalized parabolic waveform with peak voltage of 6V is split into 10 pieces and applied into PolM. The simulation results are given in Fig.4 (b). As can be seen, the time duration remains unchanged, while the chirp rate and bandwidth increase to 0.185 GHz/ns and 2.35 GHz, respectively, corresponding to the TBWP of 30. The PSR is about 6.81 dB. The FWHM is 0.524 ns, corresponding to a PCR of 24.4. The RFSSR is about 19.1 dB. Thus, splitting parabolic signal can effectively improve the performance of generated chirp signal.

Besides, from Fig. 4(b_iv), we can see several weak lines are around the instantaneous frequency line, which is mainly caused by the split of the parabolic waveform. In Eq. (10), a_n has no effect on the instantaneous frequency after differential operation. But as $2\beta a_n$ is not adjusted to $2k\pi$ (k is integer), many discontinuity points may appear around the phase curve, which is the main factor for the harmonic frequencies occurrence.

Thence, we adjust peak voltage of the parabolic signal to 8V, and the simulation results are shown in Fig. 5(a). Compared with the results in Fig. 4(b), the bandwidth, chirp rate and the carrier frequency remain unchanged, while clutters are obviously reduced in Fig.5 (b_ii), weak lines are disappeared in Fig.5 (b_iv), and the RFSSR increases to 42.1 dB.

In another study, the normalized parabolic waveform with fixed peak voltage of 8 V and time duration of 12.8 ns is split into 80 pieces. Then the splitting parabolic signal is applied to drive the PolM. The parabolic waveform, spectrum, waveform, instantaneous frequency, auto-correlation of the generated current are given in Fig. 5(b). From Fig. 5(b), we can know the chirped signal have a bandwidth of 25 GHz, and a chirp rate of 1.95 GHz/ns, corresponding to a TBWP of 320. After pulse compression, the auto-correlation function have the FWHM of 0.0467 ns, and PSR of 6.96 dB. The corresponding PCR can be calculated to 274.

Fig.6 presents the RFSSR as a function of the peak voltage V_s under different splitting pieces N. As expected, the maximum RFSSR will be obtained by adjusting V_s to 8 V or 16 V, and lower RFSSR will appear as $V_s$in other voltages. Low voltages (V_s <4V) have deteriorating RFSSR, which is mainly for the harmonic components with 40 GHz RF signal. As the peak voltage V_s is 12 V, a_n of splitting parabolic waveform will cause π phase shift in the chirped waveform, and the worst RFSSR will appear in the electrical spectrum. Thus, amplitude control of parabolic waveform is critical to the performance of the generated signal.

Therefore, splitting parabolic waveform offers an effective strategy for chirped signal generation with large bandwidth, and signal performance can be further enhanced by increasing the number of the splitting piece. After carefully controlling the parabolic waveform to make $V_s = 2V_{\pi 2}$, chirped signal with increased TBWP and high RFSSR can be generated.

B. SPLITTING AND PHASE-ENCODING PAREBOLIC WAVEFORM

The bandwidth of the generated chirp signal can be improved by splitting parabolic waveform. After phase-encoding the parabolic waveform, chirped signal with large TBWP can be achieved. First, AWG is employed to generate a 13-bit binary phase-coded parabolic waveform, corresponding to the convolution results between parabolic signal and 13-bit Barker codes. One bit parabolic waveform has a time duration of 25.6 ns, peak voltage of 8 V, and split piece of 10. The waveform is shown in Fig. 7(a_i) and applied to drive the PolM. As can be seen, convolution result causes a 4V difference between the higher and the lower waveform, which is equal to $V_{\pi 2}$. $V_{\pi 2}$ changes in parabolic waveform will introduce a π phase shift in the generated chirp waveform. The electrical spectrum is shown in Fig. 7(a_ii), and the RFSSR is 39.03 dB. The waveform of the generated signal is shown in Fig. 7(a_iii). The instantaneous frequencies in dotted lines are shown in Fig. 7(a_iv) and (a_v). As can be seen, the bandwidth of the generated signal is 1.56 GHz, and the temporal duration increases to 332.8 ns, corresponding to a TBWP of 519. And at 25.6 ns in Fig. 7(a_v), the instantaneous frequency is extended, which is mainly due to the π phase shift in the waveform. After coherent demodulation with 40 GHz, baseband signal is shown in Fig.7 (a_vi), and zoom-in views of the demodulated waveform in the dotted lines are presented in Fig.7 (a_vii). As can be seen in the two time durations, the waveform has opposite polarity, while other parameters remain unchanged. Thus a phase-coded chirped microwave

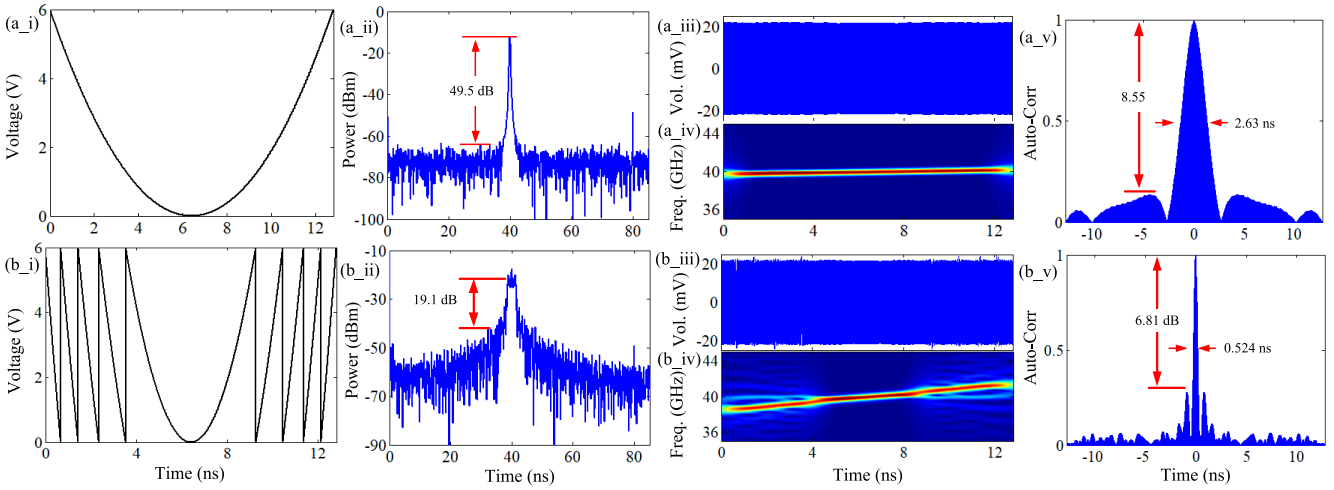

FIGURE 4. The parabolic waveforms, electronic spectra, generated chirped waveforms, instantaneous frequencies and auto-correlation functions with different split numbers when the peak voltage of the parabolic signal is 6V. (a) N = 1, (b) N = 10.

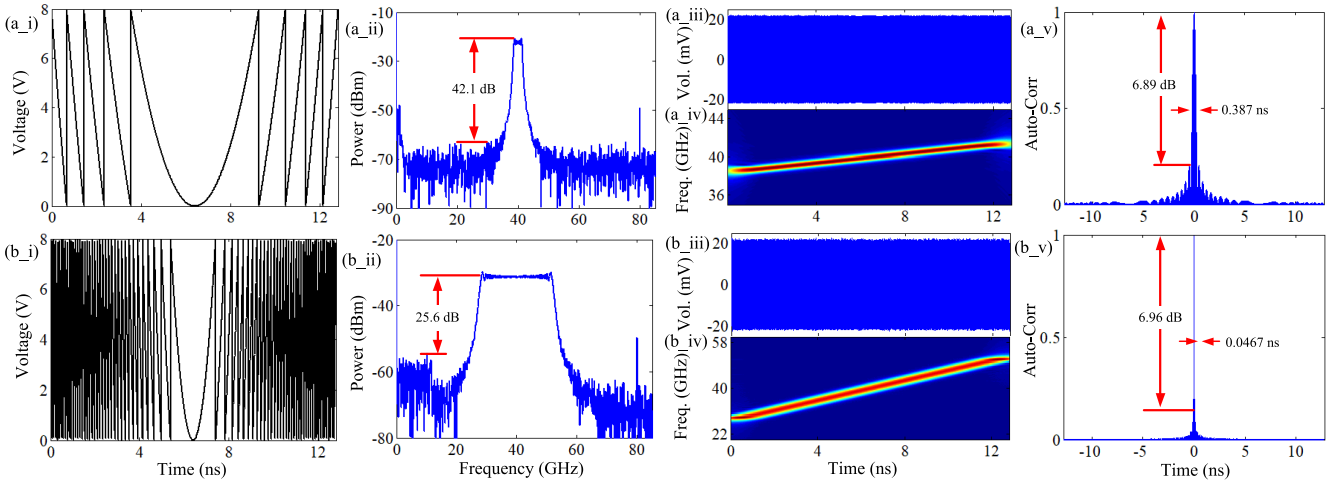

FIGURE 5. The parabolic waveforms, electrical spectra, generated chirped waveforms, instantaneous frequencies and auto-correlation functions with different split numbers when the peak voltage of the parabolic signal is 8v. (a) N = 10, (b) N = 80.

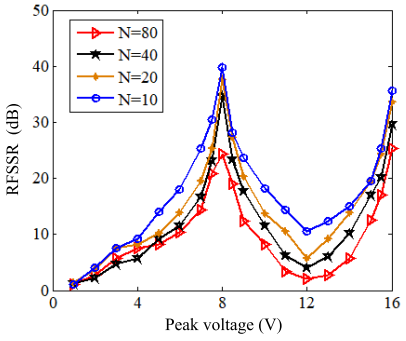

FIGURE 6. RFSSR as a function of peak voltage V_s with different split numbers.

waveform is generated, and the auto-correlation result of the chirped waveform is given in Fig.7 (a_viii). The PSR is 11.4 dB. The FWHM reduces to 0.725 ns, corresponding to a PCR of 459.

To further improve the TBWP, 63-bit PN sequence is adopted to phase-encode the parabolic waveform. One bit parabolic waveform has a time duration of 25.6 ns, peak voltage of 8V, and split piece of 80. According to Eq. (18), the theoretical value of TBWP can be calculated to 20160. The simulation results are shown in Fig.7 (b). Compared with Fig. 7 (a), the bandwidth increases to 12.5 GHz, the chirp rate improves to 0.488 GHz/ns, and the temporal duration increases to 1.6128 μs. The TWBP can be calculated to 20160, which consistent well with the theoretic analysis. The demodulation waveform in dotted lines are shown in Fig.7 (b_vii) and (b_iii), which have opposite polarity in the two time durations. Fig.7 (b_ix) shows the auto-correlation result of the obtained chirp waveform with the quasi-matched filter to enhance sidelobe ratio. The PSR increases to 18.3 dB, the FWHM is about 0.0891, and the PCR can be calculated to 18092.

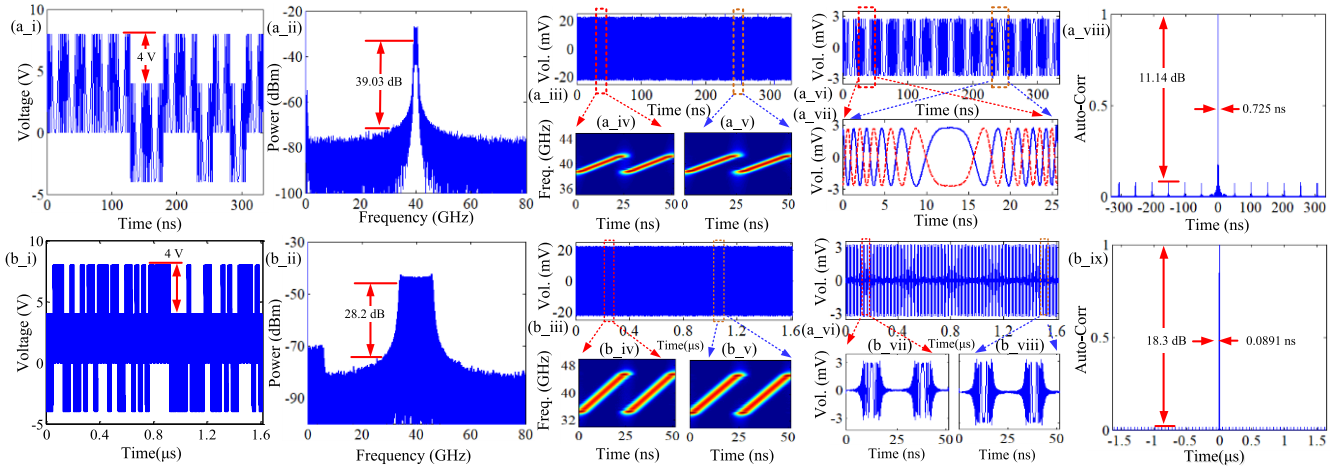

FIGURE 7. The parabolic waveforms, electronic spectra, generated chirped waveforms, instantaneous frequencies in dotted lines, coherent demodulation with 40 GH, waveforms in dotted lines and auto-correlation functions with different PN lengths and spilt numbers when $T_0 = 25.6$ ns. (a) N = 10, M = 13; (b) N = 80, M = 63.

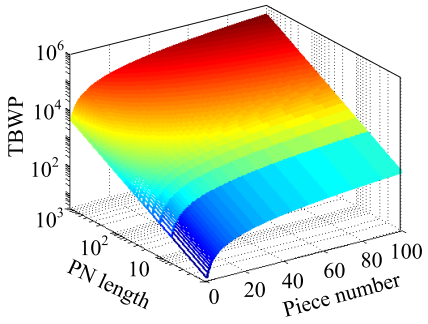

FIGURE 8. TBWP varies with PN length and splitting number.

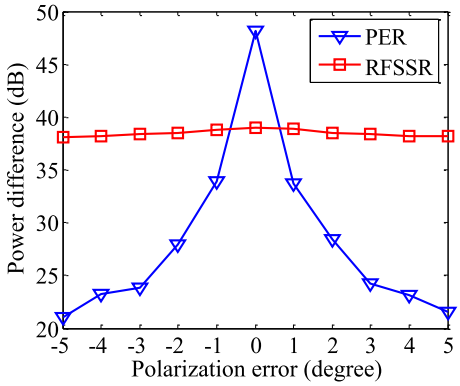

FIGURE 9. PER and RFSSR varies with polarization error.

Fig.8 presents the TBWP as a function varying with the PN length M and piece number N. As expected, the TBWP can be improved by employing long PN sequence and high piece number. Besides, for radar observation scenes with fixed pulse duration, TBWP can be improved by increasing the piece number; for fixed bandwidth scenes, long PN length can be used to enhance the TBWP. Therefore, the proposed approach can generate chirped signal with increased TWBP, and guarantee independent tunability of time width and bandwidth.

As N and M are respectively set to 10 and 13, the impact of the non-ideal polarization rotation of PC2 on PER and RFSSR are shown in Fig.9. It can be seen, the PER increases with polarization error ($|\Delta\alpha|$), while the RFSSR is almost unchanged at 39 dB, which consists well with the previous analysis in Eq. (11) and (12). As the polarization error is less than 5 degree, the structure can guarantee the PER higher than 21 dB and the RFSSR at 35 dB. Thus the proposed approach has good stability in chirped signal generation.

C. REMOTE FIBER TRANSMISSION OF CHIRPED SIGNAL WITH INCREASED TBWP

When the modulated optical signal propagates to a remote base station, phase shift will be introduced by the dispersion in fiber. In this simulation, the normalized parabolic waveform with fixed peak voltage of 8 V and time duration of 12.8 ns is phase-encoded with 13-bit Baker code, and applied to drive the PolM. The waveform of the binary phase-coded parabolic signal is shown in Fig. 9 (i).The transmission link employs a 35 km SMF. The SMF has a group velocity dispersion of -20 ps^2/km and an attenuation of 0.2 dB/km. After detection in PD, the electrical spectrum of the generated signal is shown in Fig.9 (ii). Due to the dispersion impact, harmonic frequencies at 20 GHz and 60 GHz appear, which can be effectively restrained by employing a DPol-MZM with high extinction ratio. After bandpass filter, the waveform at 40 GHz is shown in Fig. 9(ii). As can be seen, dispersion and attenuation in fiber affect the initial phase and peak voltage of the generated signal respectively. And the initial phase can be flexibly adjusted by the PC3, as shown in Fig. 9(vi).

Fig.10 presents the power of the chirped signal as a function varying with the fiber distance under difference split pieces and code numbers. As can be seen, the powers reduce proportionally with distance, which is mainly for

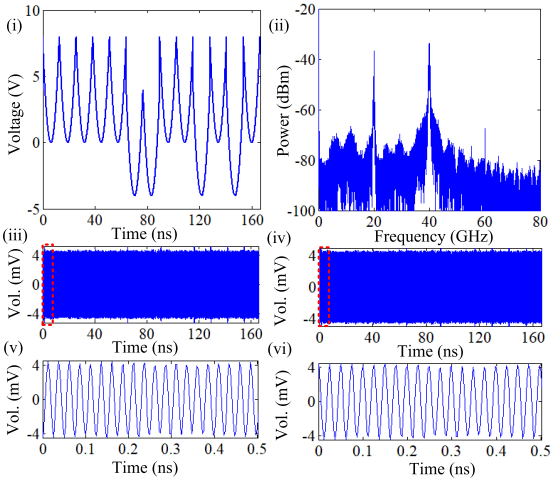

FIGURE 10. The parabolic waveform (i), electronic spectrum (ii), generated chirped waveform before (iii) and after (iv) PC adjusting, (v) and (vi) waveform in dotted lines over 35 km SMF.

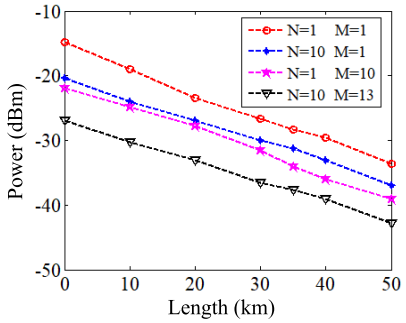

FIGURE 11. Power of the generated signal as a function of fiber length with different PN lengths and spilt numbers.

the attenuation in fiber, and the dispersion has no impact on the power of the generated signal. Thus, since the two orthogonally-polarized wavelengths are employed, the proposed scheme can avoid the periodic power fading problem caused by dispersion.

Notably, Eq. (22) simplifies the extended sidebands to $+1$-st and -1-st sidebands dispersion analysis, which applies to conventional parabolic signal and small split number. However, as the spilt number increases, the bandwidth of the extended sidebands will be further broadened, and the dispersion analysis of Eq. (22) is no longer applicable. The broadband spectra have specific dispersions at different frequency components. Different dispersions affect the phase value of the generated chirp signal. The phase value have no effect on the linearity of the chirped signal after differentiation, while the electrical spectrum will be expanded and even deteriorated into distortion. Thus, the long-distance dispersion-suppression transmission of chirped signal with large bandwidth should be investigated in the further research.

Therefore, linearly chirped microwave waveforms with large TBWP are obtained in the proposed scheme. The improvement of TBWP can overcome the contradiction between detection range and range accuracy, and improve the track performance in radar system [32]. Chirped signal with high PCR can reduce the interference and concealment of the sidelobe on the reflected echo of the weak signal. The usage of orthogonally-polarized wavelengths can effectively avoid dispersion impact from the remote BS. In practical application, filed programmable gate array (FPGA) can be employed to generate the parabolic waveform [33], [34]. Besides, the proposed system may suffer from the DC bias-drifting problem for the usage of DPol-MZM, which can be effectively solved by adding automatic bias controller in the structure.

Moreover, linearly chirped signal adopts simple frequency modulation scheme, which will be easily intercepted by non-cooperative radars, even enemy radar systems [35]. As radar system adopts hybrid frequency/phase modulation signal, low probability of intercept (LPI) performance will be significantly improved [36], [37]. Thus, the phase-coded chirped signal offers advantages such as large TBWP, high detection resolution, anti-interference and low-interception characteristics, which provides a good strategy for LPI radar system in complex dense electromagnetic environment.

IV. CONCLUSION

In summary, we have proposed and investigated a photonic approach to generate and transmit the chirped signal based on DPol-MZM and PolM. The proposed approach increases the bandwidth by splitting parabolic waveform, improves the temporal duration by phase-encoding the waveform, and adjusts the initial phase by controlling PC3. The feasibility of the approach is verified by simulations. The simulation results show the central frequency is increased to 40 GHz, the bandwidth is improved to 12.5 GHz, and the temporal duration is increased to 1.6128 μs, corresponding to an increased TBWP of 20160. The sidelobes are effectively suppressed by using the generated chirp signals, and the harmonic components can be effectively restrained by properly adjusting parabolic amplitude. The structure shows good stability for the toleration of polarization error. Thus, radar detection performance can be enhanced by using the generated signal. The proposed system offers four key advantages simultaneously, to generate chirped signal with large TBWP, to realize independent tunability of time width and bandwidth, to conduct frequency and bandwidth multiplying operation, to guarantee constant initial phase. The generator features filter-free, good tunability and reconfigurable signal generation, which provides an effective strategy for the increased-TWBP modern radar systems.

REFERENCES

[1] C. Wang and J. Yao, "Chirped microwave pulse compression using a photonic microwave filter with a nonlinear phase response," *IEEE Trans. Microw. Theory Techn.*, vol. 57, no. 2, pp. 496–504, Feb. 2009.

[2] M. I. Skolnik, Ed., *Radar Handbook*, 2nd ed. New York, NY, USA: McGraw-Hill, 1991.

[3] X. Wang, J. Ma, S. Huang, and Q. Zhang, "Generation of frequency septupled chirped microwave waveforms with increased TBWP based on two cascaded polarization modulators," *Opt. Commun.*, vol. 424, pp. 1–6, Oct. 2018.

[4] L. R. Chen, "Photonic generation of chirped microwave and millimeter wave pulses based on optical spectral shaping and wavelength-to-time mapping in silicon photonics," *Opt. Commun.*, vol. 373, no. 1, pp. 70–81, Aug. 2016.
[5] A. M. Kawalec, "SAW dispersive delay lines in radar signal processing," in *Proc. IEEE Int. Radar Conf.*, May 1995, pp. 732–736.
[6] J. Capmany and D. Novak, "Microwave photonics combines two worlds," *Nature Photon.*, vol. 1, no. 6, pp. 319–330, Apr. 2007.
[7] J. Capmany, J. Mora, I. Gasulla, J. Sancho, J. Lloret, and S. Sales, "Microwave photonic signal processing," *J. Lightw. Technol.*, vol. 31, no. 4, pp. 571–586, Feb. 15, 2013.
[8] T. Wu, C. Zhang, H. Zhou, H. Huang, and K. Qiu, "Photonic microwave waveforms generation based on frequency and time-domain synthesis," *IEEE Access*, vol. 6, pp. 34372–34379, 2018.
[9] A. Krishnan, M. Knapczyk, L. G. de Peralta, A. A. Bernussi, and H. Temkin, "Reconfigurable direct space-to-time pulse-shaper based on arrayed waveguide grating multiplexers and digital micromirrors," *IEEE Photon. Technol. Lett.*, vol. 17, no. 9, pp. 1959–1961, Sep. 2005.
[10] J. D. McKinney, D. E. Leaird, and A. M. Weiner, "Millimeter-wave arbitrary waveform generation with a direct space-to-time pulse shaper," *Opt. Lett.*, vol. 27, no. 15, pp. 1345–1347, Aug. 2002.
[11] M. Shen and R. A. Minasian, "Toward a high-speed arbitrary waveform generation by a novel photonic processing structure," *IEEE Photon. Technol. Lett.*, vol. 16, no. 4, pp. 1155–1157, Apr. 2004.
[12] P. Zhou, F. Zhang, Q. Guo, and S. Pan, "Linearly chirped microwave waveform generation with large time-bandwidth product by optically injected semiconductor laser," *Opt. Express*, vol. 24, no. 15, pp. 18460–48467, Jul. 2016.
[13] C. Wang and J. Yao, "Large time-bandwidth product microwave arbitrary waveform generation using a spatially discrete chirped fiber Bragg grating," *J. Light. Technol.*, vol. 28, no. 11, pp. 1652–1660, Jun. 1, 2010.
[14] H. Gao, C. Lei, M. Chen, F. Xing, H. Chen, and S. Xie, "A simple photonic generation of linearly chirped microwave pulse with large time-bandwidth product and high compression ratio," *Opt. Express*, vol. 21, no. 20, pp. 23107–23115, 2013.
[15] H. Zhang, W. Zou, and J. Chen, "Generation of a widely tunable linearly chirped microwave waveform based on spectral filtering and unbalanced dispersion ," *Opt. Lett.*, vol. 40, no. 6, pp. 1085–1088, 2015.
[16] A. Rashidinejad and A. M. Weiner, "Photonic radio-frequency arbitrary waveform generation with maximal time-bandwidth product capability," *J. Lightw. Technol.*, vol. 32, no. 20, pp. 3383–3393, Oct. 15, 2014.
[17] M. Li and J. Yao, "Photonic generation of continuously tunable chirped microwave waveforms based on a temporal interferometer incorporating an optically pumped linearly chirped fiber Bragg grating," *IEEE Trans. Microw. Theory Techn.*, vol. 59, no. 12, pp. 3531–3537, Dec. 2011.
[18] P. Ghelfi, F. Scotti, F. Laghezza, and A. Bogoni, "Photonic generation of phase-modulated RF signals for pulse compression techniques in coherent radars," *J. Lightw. Technol.*, vol. 30, no. 11, pp. 1638–1644, Jun. 1, 2012.
[19] W. Li, W. T. Wang, W. H. Sun, L. X. Wang, and N. H. Zhu, "Photonic generation of arbitrarily phase-modulated microwave signals based on a single DDMZM," *Opt. Express*, vol. 22, no. 7, pp. 7446–7457, Apr. 2014.
[20] Y. Li, A. Dezfooliyan, and A. M. Weiner, "Photonic synthesis of spread spectrum radio frequency waveforms with arbitrarily long time apertures," *J. Lightw. Technol.*, vol. 32, no. 20, pp. 3580–3587, Oct. 15, 2014.
[21] H. Deng, J. Zhang, X. Chen, and J. Yao, "Photonic generation of a phase-coded chirp microwave waveform with increased TBWP," *IEEE Photon. Technol. Lett.*, vol. 29, no. 17, pp. 1420–1423, Sep. 1, 2017.
[22] Y. Zhang, X. Ye, and S. Pan, "Photonic generation of linear frequency-modulated waveform with improved time-bandwidth product," in *Proc. Int. Top. Meeting Microw. Photon. (MWP)*, Oct. 2015, pp. 1–4, Paper Web.6.
[23] Y. Zhang, X. Ye, Q. Guo, F. Zhang, and S. Pan, "Photonic generation of linear-frequency-modulated waveforms with improved time-bandwidth product based on polarization modulation," *J. Lightw. Technol.*, vol. 35, no. 10, pp. 1821–1829, May 15, 2017.
[24] H. Yamazaki, T. Yamada, T. Goh, and A. Kaneko, "PDM-QPSK modulator with a hybrid configuration of silica PLCs and $LiNbO_3$ phase modulators," *J. Lightw. Technol.*, vol. 29, no. 5, pp. 721–727, Mar. 1, 2011.
[25] Y. Mei *et al.*, "Photonic generation of chirped microwave signals with high time-bandwidth product," *Opt. Commun.*, vol. 316, pp. 106–110, Apr. 2014.
[26] S. Zhu, M. Li, N. H. Zhu, and W. Li, "Transmission of dual-chirp microwave waveform over fiber with compensation of dispersion-induced power fading," *Opt. Lett.*, vol. 43, no. 11, pp. 2466–2469, Jun. 2018.
[27] W. Li and J. Yao, "Generation of linearly chirped microwave waveform with an increased time-bandwidth product based on a tunable optoelectronic oscillator and a recirculating phase modulation loop," *J. Lightw. Technol.*, vol. 32, no. 20, pp. 3573–3579, Oct. 15, 2014.
[28] J. Zhang, O. L. Coutinho, and J. Yao, "A photonic approach to linearly chirped microwave waveform generation with an extended temporal duration," *IEEE Trans. Microw. Theory Techn.*, vol. 64, no. 6, pp. 1947–1953, Jun. 2016.
[29] A. M. Haimovich, R. S. Blum, and L. J. Cimini, "MIMO radar with widely separated antennas," *IEEE Signal Process. Mag.*, vol. 25, no. 1, pp. 116–129, Dec. 2007.
[30] J.-W. Shi, F.-M. Kuo, N.-W. Chen, S. Y. Set, C.-B. Huang, and J. E. Bowers, "Photonic generation and wireless transmission of linearly/nonlinearly continuously tunable chirped millimeter-wave waveforms with high time-bandwidth product at W-band," *IEEE Photon. J.*, vol. 4, no. 1, pp. 215–223, Feb. 2012.
[31] J. P. Yao, F. Zeng, and Q. Wang, "Photonic generation of ultrawideband signals," *J. Lightw. Technol.*, vol. 25, no. 11, pp. 3219–3235, Nov. 2007.
[32] D. Zhu and J. Yao, "Dual-chirp microwave waveform generation using a dual-parallel Mach-Zehnder modulator," *IEEE Photon. Technol. Lett.*, vol. 27, no. 13, pp. 1410–1413, Jul. 1, 2015.
[33] H.-F. Zhang *et al.*, "High-speed arbitrary waveform generator based on FPGA," in *Proc. IEEE Nucl. Sci. Symp. Med. Imag. Conf. (NSS/MIC)*, Oct./Nov. 2014, pp. 1–5.
[34] T. Alpert *et al.*, "Arbitrary waveform generator based on FPGA and high-speed DAC with real-time interface," in *Proc. 8th Conf. Ph.D. Res. Microelectron. Electron.*, Jun. 2012, pp. 1–4.
[35] D. C. Schleher, "LPI radar: Fact or fiction," *IEEE Aerosp. Electron. Syst. Mag.*, vol. 21, no. 5, pp. 3–6, May 2006.
[36] M. Kowatsch and J. Lafferl, "A spread-spectrum concept combining chirp modulation and pseudonoise coding," *IEEE Trans. Commun.*, vol. 31, no. 10, pp. 1133–1142, Oct. 1983.
[37] A. Roy, H. B. Nemade, and R. Bhattacharjee, "Performance of multiuser communication system using phase coded linear chirp modulation," in *Proc. 23rd Nat. Conf. Commun. (NCC)*, Mar. 2017, pp. 1–6.

KUN ZHANG received the B.S. and M.S. degrees from Air Force Engineering University, Xi'an, China, in 2014 and 2016, respectively, where he is currently pursuing the Ph.D. degree. His research interests include microwave photonics, board optical signal processing, and multi-band radar systems.

SHANGHONG ZHAO received the bachelor's and master's degrees from the Physics Department, Lanzhou University, Lanzhou, China, in 1984 and 1989, respectively, and the Ph.D. degree from the Xi'an Institute of Optics and Precision Mechanics, CAS, in 1998. He is currently a Full Professor with Air Force Engineering University, Xi'an, China. He is also the Head of the Space Based Information Network Research Center. He has authored over 300 academic articles and four books. His teaching interests are in fields of microwave photonics, space-based information networks, quantum key distribution, and optoelectronics.

YUFU YIN received the B.S. and M.S. degrees from Air Force Engineering University, Xi'an, China, in 1989 and 1992, respectively, where he is currently a Full Professor. He is also the Dean of the Information and Navigation College.

TAO LIN received the B.S. and M.S. degrees from Air Force Engineering University, Xi'an, China, in 2015 and 2017 respectively, where he is currently pursuing the Ph.D. degree. His research interests include microwave photonics and satellite optical communication.

XUAN LI received the bachelor's, master's, and Ph.D. degrees from Air Force Engineering University, Xi'an, China, in 2011, 2014, and 2017, respectively, where he is currently an Associate Professor. His current research interests include microwave photonics and UWB radar signal generation.

WEI JIANG received the bachelor's and master's degrees from Air Force Engineering University, Xi'an, China, in 2004 and 2007, respectively, where she is currently pursuing the Ph.D. degree. She is also a Senior Engineer with the National Key Laboratory of Science and Technology on Space Microwave, Xi'an. Her research interests include optical satellite networks, on-board optical signal processing, and microwave photonics.

GUODONG WANG received the B.S. degree from Air Force Engineering University, Xi'an, China, in 2017, where he is currently pursuing the M.S. degree. His research interests include microwave photonics and microwave signal processing.